ACS APPLIED MATERIALS & INTERFACES

www.acsami.org

Research Article

Putting Forward NUS-8-CO_2H/PIM-1 as a Mixed Matrix Membrane for CO_2 Capture

Dong Fan,[†] Aydin Ozcan,[†] Naseem A. Ramsahye, Guillaume Maurin, and Rocio Semino*

Cite This: *ACS Appl. Mater. Interfaces* 2022, 14, 16820−16829

Read Online

ACCESS | Metrics & More | Article Recommendations | Supporting Information

ABSTRACT: Mixed matrix membranes (MMMs) composed of NUS-8 metal−organic framework (MOF) nanosheets dispersed into a polymer of intrinsic microporosity 1 (PIM-1) polymer matrix are known to be promising candidates for CO_2/N_2 separation because of a solubility-driven separation mechanism. In this work, we predict that a chemical functionalization of the organic linker of NUS-8 by a CO_2-philic function confers an even better separation performance to the resulting MMM. Our simulations revealed that the NUS-8-CO_2H/PIM-1 composite exhibits a 3-fold increase in CO_2/N_2 selectivity versus the NUS-8/PIM-1 analogue while achieving a high CO_2 permeability (6700 barrer). We demonstrated that this improved level of performance is due to an increase both in the total MOF/polymer interfacial pore volume and in the CO_2-affinity due to the chemical functionalization. These results suggest that an appropriate choice of chemical functionalization of a MOF is a promising strategy to improve gas separation performances for MMM composites that exhibit a solubility-driven separation mechanism.

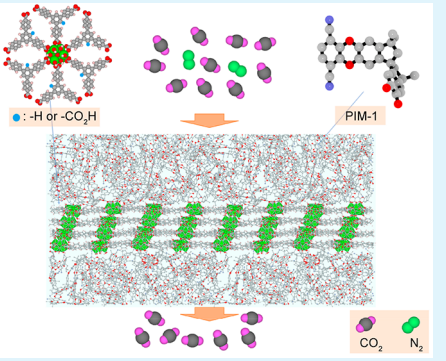

KEYWORDS: *adsorption, metal−organic frameworks, polymer-based mixed matrix membranes, Monte Carlo, non-equilibrium molecular dynamics*

Downloaded via UNIV MONTPELLIER on February 1, 2023 at 12:51:52 (UTC).
See https://pubs.acs.org/sharingguidelines for options on how to legitimately share published articles.

1. INTRODUCTION

Membranes are a promising green-technology alternative to the currently used energy-demanding gas separation techniques owing to their small footprint, low energy consumption, and ease of operation.[1,2] For example, membrane technology addresses two key CO_2 capture processes associated with CO_2/CH_4 (precombustion) and CO_2/N_2 (postcombustion) separations. Polymeric membranes were first developed to this end; however their separation performance suffers from a permeability/selectivity trade-off, termed the "Robeson upper bound".[3] Indeed, permeability must be sacrificed for selectivity and vice versa, and this considerably reduces the attractiveness of most polymeric membranes for processing huge amounts of gases in industrial plants. In order to overcome the Robeson upper bound, alternative membrane technologies have been proposed, such as the incorporation of selective porous materials into the polymeric matrix as fillers to form mixed matrix membranes (MMMs). Many different inorganic, organic, and organic/inorganic fillers have been considered, e.g., zeolites,[4] carbon-based nanotubes,[5] graphene oxides,[6] and metal−organic frameworks (MOFs),[1] among others.[7] The latter can be tuned in terms of their pore size/shape and chemical functionalities, which enables modulation of the adsorptive and diffusive properties for a range of guest molecules.[8−10] A series of MMMs with enhanced separation selectivity and/or gas permeability for a wide range of gas mixtures compared with pure polymers have been developed by combining MOFs with processable polymeric matrices.[9,11−17]

Functionalizing MOFs, polymers, or both components in MMMs has been envisaged as a promising strategy not only to obtain a good interfacial compatibility between the two components for the fabrication of continuous and mechanically stable membranes[18−21] but also to tune their performance.[22−28] Specifically, Ghalei et al. reported an enhancement in CO_2/N_2 selectivity for the NH_2 functionalized UiO-66-NH_2(Zr)/PIM-1 MMM compared with the pristine UiO-66(Zr)/PIM-1 analogue (from 14 to 25 at 20 wt % loading), at the expense of a drastic reduction of the gas permeability by about 30%.[22] On another work, Ahmad et al.[27] evidenced that the ligand functionalization of UiO-66(Zr) by NH-$COCH_3$ groups only slightly increases the CO_2/CH_4 selectivity of the corresponding UiO-66-NH-$COCH_3$/6FDA-DAM MMM as compared with its pristine UiO-66(Zr) analogue (33 vs 31) again associated with a decrease of the CO_2 permeability (1263 barrer vs 1912 barrer). A similar permeability/selectivity trade-off was reported by Liu et al.[29] for a polyethyleneimine

Received: January 3, 2022
Accepted: March 15, 2022
Published: March 29, 2022

ACS Publications

© 2022 American Chemical Society

functionalized UiO-66/6FDA-ODA MMM. More recently, Knebel et al.[12] successfully enhanced both propylene permeability and propylene/propane selectivity of a ZIF-67/6FDA-DAM MMM by functionalizing the MOF with the 1,3-bis(2,4,6-diisopropylphenyl)imidazole-2-ylidene (iDip) function.

From the polymer functionalization side, Carja et al.[21] revealed that while PIM-1 functionalized with amidoxime ensures an improvement of the adhesion with UiO-66 in the corresponding MMM, it also induces a significant drop of gas permeability compared with the UiO-66/PIM-1 analogue. Tien-Binh et al.[20] demonstrated that functionalizing both MOF (MIL-53 with $-NH_2$ groups) and polymer (6FDA-DAM-HAB with $-OH$ functions) components leads to an increase of the CO_2/CH_4 selectivity from 2.2 to 5.1 for the resulting MMM while maintaining comparable CO_2 permeability. In another study, Wang et al.[26] functionalized UiO-66(Zr) with $-NH_2$ groups and PIM-1 with amidoxime and reported an improvement for both CO_2/CH_4 (23.0 vs 12.3) and CO_2/N_2 (27.5 vs 15.6) selectivities vs UiO-66(Zr)/PIM-1 combined with a rather high CO_2 permeability of 8425 barrer. Other works have considered functionalization as a strategy to improve gas permeability at the expense of decreasing the selectivity.[30] For example, Amedi et al.[31] managed to improve the CO_2 permeability of the ZIF-8/PEBA MMM by a factor of 2 with the aminosilane-functionalized ZIF-8 while keeping the CO_2/CH_4 selectivity at the same level (~16).

NUS-8 nanosheets composed of $Zr_6O_4(OH)_4$ and 1,3,5-benzenetribenzoate (BTB) are very promising fillers for shape-selective applications, as they combine in-plane porosities with high chemical stability.[32] The uniformly dispersed MOF nanosheets in a polymeric matrix are also expected to provide fast transport pathways through both internal pores and internanosheet channels. The NUS-8/PIM-1 composite exhibits promising CO_2 separation performances with a rather high CO_2/N_2 selectivity of 11 while achieving high permeability values.[33] In previous work, we proposed a molecular-level explanation of this phenomenon: the presence of microvoids at the MOF/polymer interface provides a highway[34] between the polymer and the MOF, leading to an effective solubility-driven separation mechanism.[33] Herein, we propose to incorporate CO_2-philic functional groups into the NUS-8 fillers with the aim of enhancing the solubility-dominated separation performances of the resulting PIM-1 based MMM. We deliberately selected the $-CO_2H$ function because it has been demonstrated to boost the CO_2 affinity for a range of functionalized MOFs.[34,35] As a starting point, we combined density functional theory (DFT) calculations with force field-based Monte Carlo (MC) simulations to assess the impact of the $-CO_2H$ functionalization of NUS-8 on its CO_2/N_2 thermodynamic separation properties. We further built an atomistic model of the NUS-CO_2H/PIM-1 composite[36] by combining DFT calculations and classical atomistic molecular dynamics (MD) simulations. We found that the functionalized composite exhibits micropores at the MOF/polymer interface of similar sizes (diameters up to 7 Å) to those previously found for the nonfunctionalized NUS-8/PIM-1,[33] but the pore size distribution maximum is shifted to larger pore sizes, leading to a substantial increase of the total pore volume. MC simulations further revealed an increase in the CO_2/N_2 thermodynamic selectivity over the whole range of pressure studied for the functionalized NUS-CO_2H/PIM-1 MMM. Finally, we investigated the gas permeability and permselectivity of the NUS-8-CO_2H/PIM-1 composite by non-equilibrium concentration-gradient driven molecular dynamics (CGD-MD) simulations. Remarkably, these simulations revealed that NUS-8-CO_2H/PIM-1 MMM exhibits a 3-fold enhancement of the CO_2/N_2 selectivity from 11 (for NUS-8/PIM-1 MMM) to 33 while achieving a high CO_2 permeability (6700 barrer) via a solubility-driven separation mechanism. We thus predict that the NUS-8-CO_2H/PIM-1 MMM is among the most promising MOF/polymer MMMs in terms of CO_2 separation performance.

2. COMPUTATIONAL METHODS

2.1. Functionalized MOF: NUS-8-CO_2H. It is known that NUS-8 can potentially adopt different stacking orders and these different stacking models in the two-dimensional nanostructures would lead to different crystal morphologies. We have previously shown that the AA stacking model has the lowest total energy when considering the experimental lattice parameters for NUS-8.[33] Here, we have also selected this stacking for the NUS-8-CO_2H model, as the functionalization of $-CO_2H$ consists of only one $-CO_2H$ group per BTB linker, so the global effect on the van der Waals interactions that dominate the NUS-8 layers' interaction should be rather small. The primitive cell of the bulk NUS-8-CO_2H structure was first optimized by DFT calculations performed via the Quickstep module of the CP2K package,[37] relying on the Perdew–Burke–Ernzerhof functional within the generalized gradient approximation (GGA) for the electronic exchange–correlation interaction.[38] All atoms except for Zr were modeled via triple-ζ plus valence polarized Gaussian-type basis sets (TZVP-MOLOPT), while for Zr double-ζ plus valence polarization functions (DZVP-MOLOPT) were employed.[39] Core electrons–valence shells interactions were described by the norm-conserving pseudopotentials proposed by Goedecker, Teter, and Hutter.[40−42] A convergence criterion of 0.01 eV $Å^{-1}$ was imposed on the atomic forces. The energy cutoff for the plane wave basis set was set to 450 Ry. The DFT-D3 van der Waals (vdW) correction method developed by Grimme was used to account for the nonbonded vdW interactions.[43] The particle positions and cell parameters were optimized until the convergence criteria were met.

The optimized NUS-8-CO_2H structure was subsequently employed to construct the NUS-8-CO_2H slab model. The NUS-8-CO_2H slab was capped considering the dissociative adsorption of the synthesis solvent, water: $-OH$ functions were added to the undercoordinated Zr atoms and the remaining $-H$ functions were considered as bonded to an O atom at the linker at the surface, as was previously done for the pristine NUS-8 surface model.[33,44] The resulting model contains four Zr-BTB layers (1056 atoms) with dimensions of 20.05 × 30.14 × 22.45 $Å^3$ (z is defined as the direction perpendicular to the slab; see Supporting Information Figure S1) and has a zero dipole in the z direction. This model was further optimized via the same computational methodology as that for the bulk NUS-8-CO_2H. Partial charges were calculated using the repeating electrostatic potential extracted atomic (REPEAT) charge method,[45] as implemented in the CP2K package.[37,46] This method is widely accepted for the computation of charges for different porous materials.[47]

The x and y directions of the final surface supercell model were duplicated to be further employed in the MD simulations (40.10 × 70.28 $Å^2$). In these simulations, the surface slab was treated as fully flexible with intramolecular potential parameters and 12−6 Lennard-Jones (LJ) site−site contributions from the universal force field (UFF).[48] Table S2 lists the vdW parameters and charges for all atom types, which are illustrated in Supporting Information Figure S2. All the force field parameters used for the functionalized NUS-8-CO_2H MOF are consistent with those employed to model the non-functionalized NUS-8 in our previous work.[33]

2.2. MOF/PIM-1 Interface Models. The NUS-8/PIM-1 interface was modeled according to our previous work.[33] In order to model the NUS-8- CO_2H/PIM-1 interface, we combined the obtained NUS-8-CO_2H surface model with a PIM-1 model[36] via MD simulations,

https://doi.org/10.1021/acsami.2c00090
ACS Appl. Mater. Interfaces 2022, 14, 16820−16829

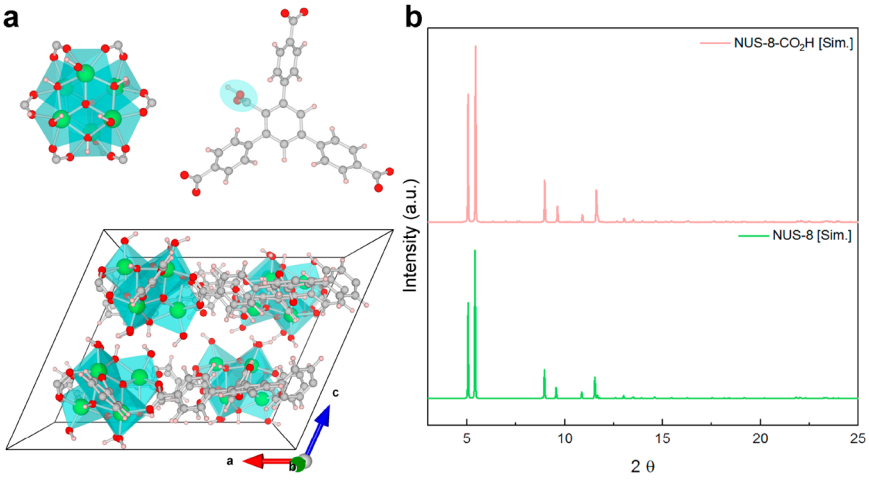

Figure 1. (a) Functionalization of the NUS-8 linker with $-CO_2H$ groups and DFT-optimized bulk structure corresponding to the AA stacking configuration. Color scheme: Zr, green; O, red; H, pink; C, gray. (b) Calculated X-ray diffraction patterns for the DFT-optimized NUS-8-CO_2H (red) and NUS-8 (green).

following the same strategy as previously done for the pristine case as well as for modeling the interfaces of a series of different MOF/polymer composites.[27,36,49] We note that the force field that we have chosen to model PIM-1[50] allows reproduction of experimental density and porosity, and it yields ideal H_2/CH_4 permselectivity data comparable to experimental data.[51] First, the atomic positions of the PIM-1 polymer model were unwrapped in the z-direction and the simulation box was adjusted according to the lattice parameters of the MOF surface models, leading to a system with dimensions of 40.39 × 70.10 × 67.74 Å^3 and 40.10 × 70.28 × 72.08 Å^3 for NUS-8/PIM-1 and NUS-8-CO_2H/PIM-1, respectively. Then, the PIM-1 model was brought into contact with the respective NUS-8 surfaces models, and the resulting composite models were subjected to an equilibration protocol consisting of 21 MD simulations integrating NVT and NP_zT cycles with T and P_z kept constant via the Berendsen thermostat and barostat[52] with relaxation times of 0.1 and 0.5 ps, respectively, in a modified version of the DL_POLY Classic code.[53] This procedure allowed for the equilibration of the PIM-1 polymer, leading to well-packed NUS-8/PIM-1 and NUS-8-CO_2H/PIM-1 interface models.[33]

The interface models were fully flexible. The interactions between NUS-8-CO_2H and PIM-1 were treated by 12−6 LJ and Coulombic potentials. The Lorentz−Berthelot mixing rules[54] were applied to compute the cross 12−6 LJ parameters. The cutoff for LJ interactions was 12 Å, and electrostatic interactions were calculated via the Ewald summation method[55] with a tolerance of 10^{-6}. Five independent simulations were carried out for each composite, each of them starting from a different PIM-1 configuration to account for the difficulty of properly sampling the whole configurational space in a single simulation trajectory.[36] Results were averaged over the five production NVT (T = 300 K) MD simulations lasting 10 ns each with a time step of 1 fs. Snapshots for the five NUS-8-CO_2H/PIM-1 independent models are shown in Supporting Information Figure S3, coupled with the corresponding pore size distribution (PSD). The PSD scatterplot was computed by employing the Zeo++ code.[56]

2.3. GCMC Simulations. Single-component and equimolar binary CO_2/N_2 mixture adsorption isotherms were calculated for both bulk NUS-8-CO_2H and the NUS-8-CO_2H/PIM-1 composite via grand canonical Monte Carlo (GCMC) simulations at 298 K. The host−guest interactions were treated by the sum of Coulomb and 12−6 LJ contributions. The electrostatic interactions were obtained via Ewald summation[55] with a 10^{-6} precision. The LJ interaction cutoff was of 12.0 Å. Each point was modeled via 1 × 10^5 MC cycles and 5 × 10^3 equilibration cycles employing the RASPA code.[57] Both bulk NUS-8-CO_2H and the NUS-8-CO_2H/PIM-1 composite were modeled using the force field parameters detailed above. CO_2 was described by the EPM2 model,[58] corresponding to three atom-centered charged LJ sites, and N_2 by a three-site model.[59] LJ cross parameters were computed via the Lorentz−Berthelot mixing rules.[54] The adsorption enthalpies were evaluated with the revised Widom's test particle insertion method.[60] This methodology was previously adopted to model the NUS-8/PIM-1 composite.[33]

The selectivity of the binary mixture isotherms was calculated according to the expression $\alpha = [y_{CO2}/y_{N2}]/[x_{CO2}/x_{N2}]$, where x_{CO2}, x_{N2} and y_{CO2}, y_{N2} are the CO_2 and N_2 concentrations in the gas phase and within the NUS-8-CO_2H or NUS-8-CO_2H/PIM-1 composites porosity, respectively. We considered an equimolar binary mixture so in our case x_{CO2}/x_{N2} = 1. Preferential interactions/locations of the guest species were evaluated via a careful inspection of the representative snapshots and quantified by several radial distribution functions between guests and composite sites averaged over all the GCMC configurations.

2.4. CGD-MD Simulations. The membrane was modeled as a NUS-8-CO_2H surface surrounded by two PIM-1 slabs that had been previously unwrapped in the z direction. Transport simulations through this membrane model were performed employing the GROMACS-2019.4 simulation package[61] and a modified version of PLUMED-2.[62] In the permeation simulations, a concentration gradient is generated between the feed and the permeate of the MMM model to create realistic non-equilibrium conditions. To achieve this goal, the density of the penetrant molecules within selected regions located at the inlet and outlet (labeled as ICR and OCR for Inlet Control Region and Outlet Control Region, respectively, in Supporting Information Figure S4) of the membrane is maintained at a target value all along the simulation. A scheme of the simulation setup and its parameters are provided in Supporting Information Figure S4 and Table S3. In these simulations, the MMM model was placed in the center of the simulation box surrounded by 10 nm void spaces at both sides along the z-direction. The MMM model atoms located up to 0.5 nm from both ends were tethered to their initial z-coordinates to prevent the membrane translation due to the concentration gradient. The total pressure in the ICR was 10 bar, while the outlet gas concentration was set to vacuum in all simulations. In a previous study we scanned different pressure ranges and showed that our simulations capture the experimental trend.[33] In this work, we kept our simulations at the single high-pressure value of 10 bar, as it represents a reasonable balance between simulation cost and accuracy. Indeed, since the permeability at low pressures is very low, the sampling improves if pressure is kept relatively high, as revealed by previous works.[63,64] Simulations were run in the NVT ensemble considering periodic boundary conditions in all directions, and the temperature was set to 300 K by a Nosé−Hoover thermostat[65] with a 0.1 ps coupling constant. The temperature of

https://doi.org/10.1021/acsami.2c00090
ACS Appl. Mater. Interfaces 2022, 14, 16820−16829

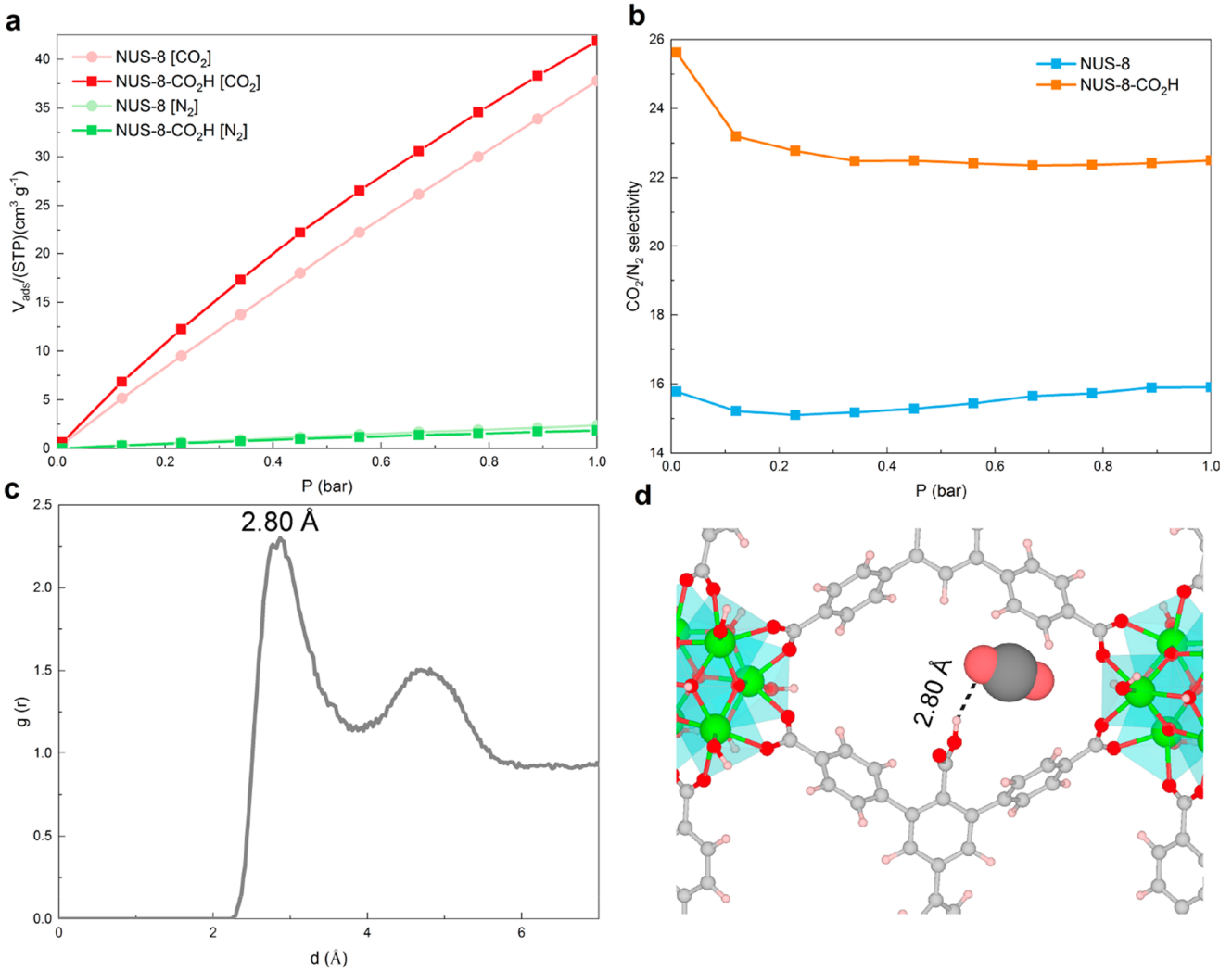

Figure 2. (a) CO_2/N_2 coadsorption isotherms (equimolar gas mixture) of the pristine NUS-8 and NUS-8-CO_2H bulk MOFs at 298 K calculated by GCMC simulations, (b) CO_2/N_2 thermodynamic selectivity as a function of pressure, (c) radial distribution function for the O_{CO_2}−$H_{NUS\text{-}8\text{-}CO_2H}$ pair (total pressure = 1 bar) and (d) illustration of the O_{CO_2}−$H_{NUS\text{-}8\text{-}CO_2H}$ interactions (color code as in Figure 1).

the gas molecules and of the different parts of the membrane was regulated by separate thermostats as previously suggested.[66] The particle mesh Ewald (PME) method[67] was employed for long-range electrostatics interactions, with a 12 Å cutoff for both the LJ and the real part of the Ewald summation. The time evolution of the system was computed via a Verlet integration algorithm with a 1 fs time step. Three independent permeation simulations were performed, each of them lasting 500 ns. The gas flux along the z-direction (J_z) corresponds to the number of molecules that cross a xy section of the membrane normalized by the simulation time (t) and the cross-sectional area of the membrane (A_{xy}):

$$J_z = \frac{N^+ - N^-}{tA_{xy}}$$

where N^+ and N^- are the number of gas molecules that cross the membrane section in the $+z$-direction (i.e., feed to permeate) and the $-z$-direction (i.e., permeate to feed), respectively. Permeability, π, is calculated according to the following transport equation:

$$\pi = \frac{J_z}{(P_{dif}/l_{memb})}$$

where P_{dif} is the pressure difference between both ends of the membrane and l_{memb} is the membrane thickness.[68] Permeation selectivity is then calculated as a ratio between permeabilities. Residence time probability distributions for each penetrant were obtained by dividing the z-direction in bins and calculating the time spent by individual molecules within each bin, regardless of its entering or leaving direction (i.e., positive and negative z-directions). Mean residence times were obtained from the residence time probability distributions.

3. RESULTS AND DISCUSSION

Figure 1a shows the DFT-optimized structure of the bulk NUS-8-CO_2H. The calculated XRD pattern of the functionalized NUS-8-CO_2H MOF shows similar Bragg peaks as those for pristine NUS-8 (see Figure 1b). The single component adsorption isotherms for CO_2 and N_2 both in NUS-8-CO_2H and NUS-8 are very similar (see Figure S5), but NUS-8-CO_2H has less adsorption capacity than pristine NUS-8 due to the reduced pore size after −CO_2H functionalization. We subsequently explored how the proposed −CO_2H functionalization of the MOF affects its CO_2 and N_2 affinities and the thermodynamic CO_2/N_2 selectivity. To this end, we carried out CO_2/N_2 coadsorption GCMC simulations on the −CO_2H functionalized MOF at 298 K and compared the results to

https://doi.org/10.1021/acsami.2c00090
ACS Appl. Mater. Interfaces 2022, 14, 16820−16829

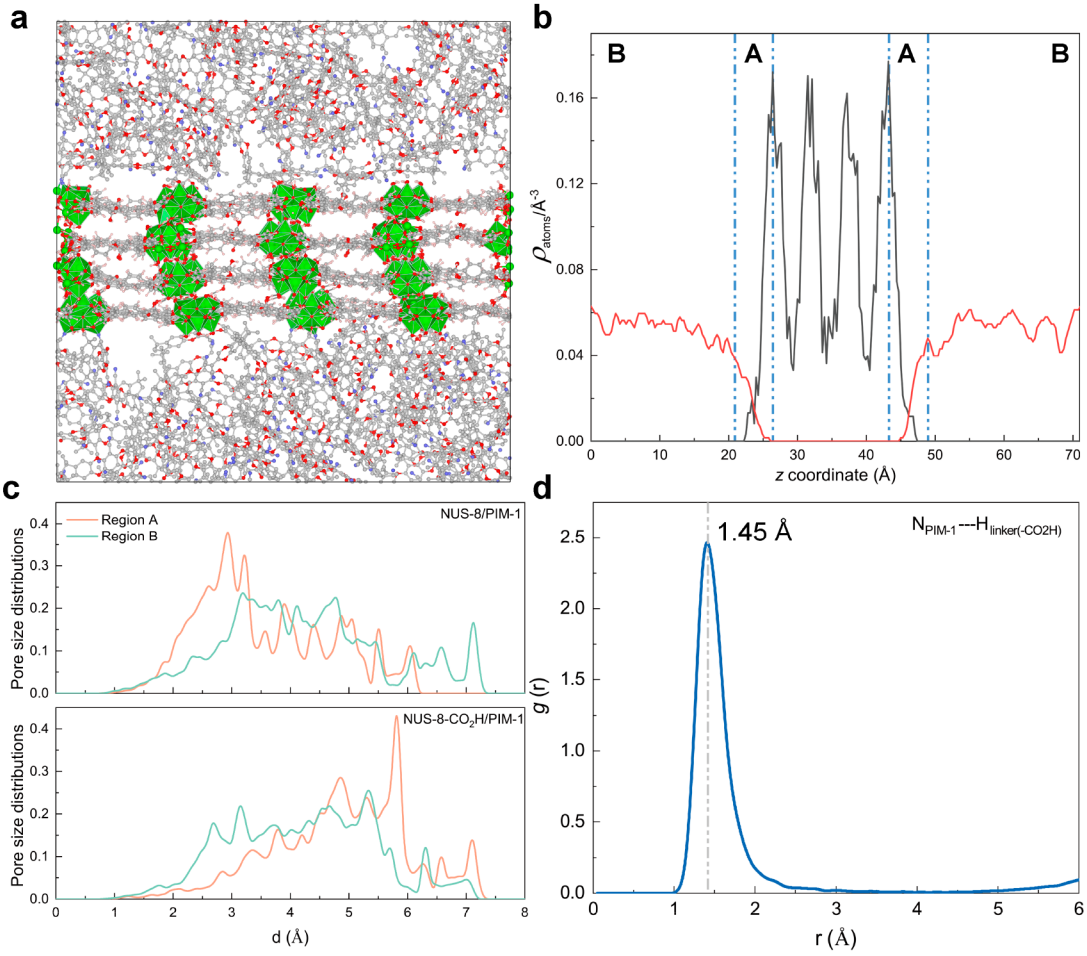

Figure 3. (a) Representative configuration of the NUS-8-CO_2H/PIM-1 composite model after 10 ns MD simulations. Color scheme: Zr, green; O, red; H, pink; C, gray; N, blue. (b) Atomic density of PIM-1 (red line) and NUS-8-CO_2H (black line) along the NUS-8-CO_2H/PIM-1 composite. (c) Pore size distributions (region A and region B) calculated for an equilibrium configuration of the NUS-8/PIM-1 (upper panel) and NUS-8-CO_2H/PIM-1 (lower panel) composites. (d) Radial distribution function between H (from the $-CO_2H$ group) of the NUS-8-CO_2H linker and the N of PIM-1.

those we previously reported for the pristine NUS-8[33] (Figure 2). The enhancement in CO_2/N_2 selectivity for the functionalized MOF compared with the pristine one (23 versus 16) can be ascribed to the O_{CO_2}−$H_{NUS\text{-}8\text{-}CO_2H}$ interaction with an associated equilibrium distance of ∼2.80 Å, as shown in Figure 2c,d. This observation confirms that the functionalization of the NUS-8 MOF by the carboxylic group leads to an increase in its affinity.

These results encouraged us to combine NUS-8-CO_2H and PIM-1 for further exploration of the properties of the corresponding composite. Figure 3a depicts a typical snapshot of the MD-equilibrated NUS-8-CO_2H/PIM-1 composite model. The NUS-8-CO_2H MOF surface is at the middle of the simulation box, surrounded by the PIM-1 polymer. Figure 3b shows the atomic density of the NUS-8-CO_2H/PIM-1 interface as a function of z-coordinate values. For PIM-1, the density fluctuates around a constant value of ∼0.056 atoms Å^{-3} in a region labeled as region B and drops to zero in close proximity to the MOF surface (labeled as region A, blue dashed-line area). PIM-1 chains do not penetrate the MOF pores. The region A section of the interface extends up to 8 ± 2 Å in the z coordinate for the NUS-8-CO_2H/PIM-1 composite. This value is an average of five independent MD simulations, and the standard deviation is assigned as the error bar. The region A length is comparable to that previously obtained for NUS-8/PIM-1, of 6 ± 2 Å.[33] Figure 3c shows the calculated pore size distribution (PSD)[56] for both regions A and B of the NUS-8-CO_2H/PIM-1 composite compared with that of the previously constructed NUS-8/PIM-1 analogue. Both composites exhibit interfacial micropores of diameters up to 7 Å, but the maximum of the pore size distribution in region A for NUS-8-CO_2H/PIM-1 (6 Å) is shifted to a larger distance compared with the nonfunctionalized MOF-based composite (3 Å). The calculated total pore volumes[69,70] of region A for NUS-8-CO_2H/PIM-1 and NUS-8/PIM-1 interface models are 0.51 ± 0.06 and 0.28 ± 0.03 cm^3 g^{-1}, respectively. These results reveal that there is an overall increase of the interfacial porosity due to a higher proportion of larger micropores.

Several site-to-site radial distribution functions (RDFs) between the MOF and the polymer were further computed from the MD simulations trajectories. The most prominent MOF/polymer interaction of the NUS-8-CO_2H/PIM-1 composite involves strong interactions between the −CN groups of PIM-1 and the $-CO_2H$ groups of NUS-8-CO_2H as shown in Figure 3d.

GCMC simulations (Figure 4a,b) further revealed that the CO_2/N_2 selectivity increases throughout the whole pressure

https://doi.org/10.1021/acsami.2c00090
ACS Appl. Mater. Interfaces 2022, 14, 16820−16829

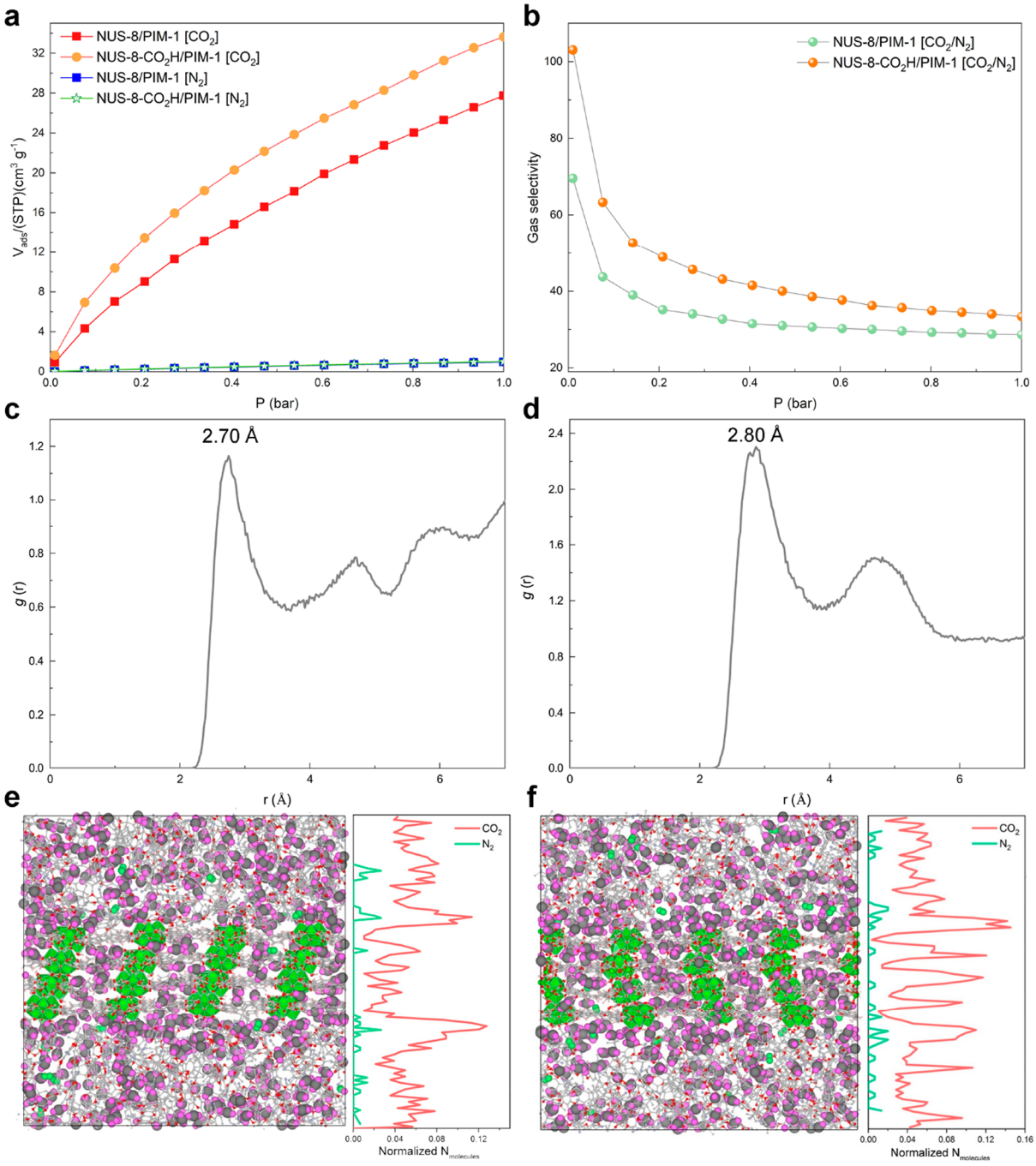

Figure 4. (a) GCMC simulated CO_2/N_2 coadsorption (equimolar binary mixture) isotherm at 298 K of NUS-8-CO_2H/PIM-1 vs NUS-8/PIM-1 and (b) CO_2/N_2 thermodynamic selectivity as a function of pressure. The adsorption isotherm for NUS-8/PIM-1 was taken from previous work.[33] (c, d) Radial distribution functions respectively displaying the interactions of CO_2 with O_{PIM-1} and $H_{-CO2H(MOF)}$ obtained from the GCMC simulations for the NUS-8-CO_2H/PIM-1 composite at 1 bar and 298 K. Snapshots showing the typical location of CO_2/N_2 in (e) NUS-8/PIM-1 vs (f) NUS-8-CO_2H/PIM-1. The number of molecules along the direction perpendicular to the MMM for the coadsorption calculations is also shown. The color scheme for the composites is the same as in Figure 3.

range for the NUS-8-CO_2H/PIM-1 composite (from 108 at 0.01 bar to 34 at 1 bar) compared with the NUS-8/PIM-1 composite (from 69 at 0.01 bar to 29 at 1 bar), as shown in Supporting Information Figure S6. This trend is also supported by an increase of the CO_2 adsorption enthalpy in NUS-8-CO_2H/PIM-1 (45.4 kJ mol^{-1}) vs NUS-8/PIM-1 (39.3 kJ mol^{-1}) while the N_2 values remain quite similar (11.5 kJ mol^{-1} vs 10.9 kJ mol^{-1}). The microscopic origin of this selectivity enhancement was further elucidated via the analysis of the host/guest interactions in the equimolar coadsorption in NUS-8-CO_2H/PIM-1. CO_2 preferentially interacts with the carboxyl group present at the NUS-8-CO_2H surface and the oxygen atom of PIM-1 in the composite (Figure 4c,d). Figure 4e,f reports the number of gas molecules normalized with respect to the number of molecules adsorbed in the bulk PIM-1 as a function of the *z* coordinate for both composites, along with an illustration of typical CO_2/N_2 locations at 1 bar. CO_2 molecules are preferentially located in the region A section

https://doi.org/10.1021/acsami.2c00090
ACS Appl. Mater. Interfaces 2022, 14, 16820−16829

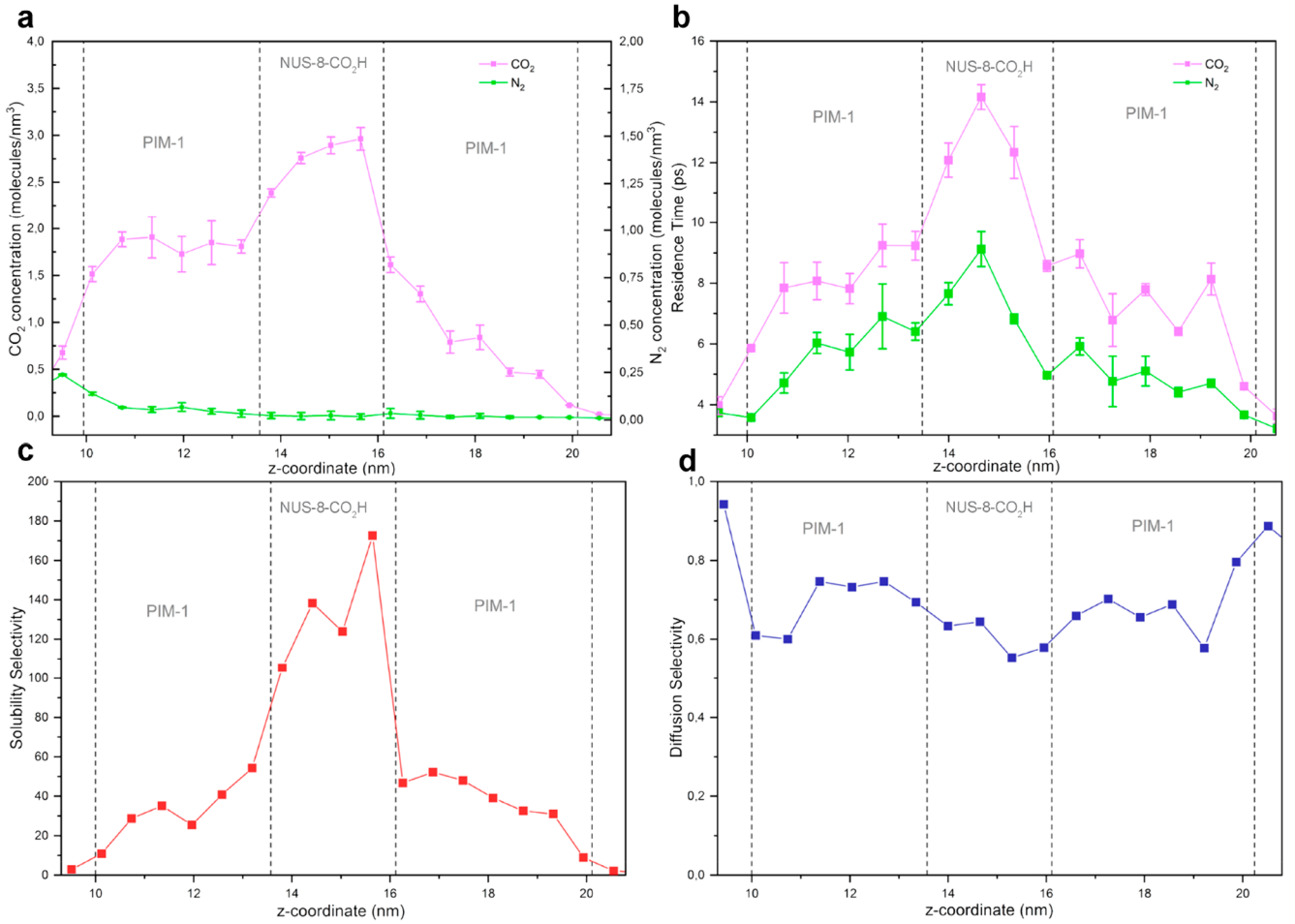

Figure 5. (a) Concentration profiles and (b) residence time distributions along the NUS-8-CO_2H/PIM-1 membrane model. Error bars are calculated as the standard deviation of the values obtained for three independent CGD-MD runs. (c, d) Solubility and diffusion contributions to the total permeation selectivity, respectively.

of the composite. In the case of the NUS-8-CO_2H/PIM-1, more CO_2 molecules are seen to accumulate within both the MOF and region A than for the case of pristine NUS-8/PIM-1 composite. The enhanced accumulation of CO_2 molecules in these regions is at the origin of the larger uptake of CO_2 molecules for the functionalized composite as compared with the NUS-8/PIM-1 counterpart (see isotherms in Figure 4a), and it can be correlated with the overall larger porosity in this composite.

We further simulated the equimolar CO_2/N_2 mixture membrane separation at 10 bar for NUS-8-CO_2H/PIM-1 using the CGD-MD method. This method enabled us to create a density gradient between the two sides of the membrane (feed and permeate) and mimic experimental conditions throughout the simulation trajectory. Remarkably, the predicted CO_2/N_2 permeation selectivity for NUS-8-CO_2H/PIM-1 (33) averaged over three independent 500 ns CGMD simulations is 3 times higher than the value we previously calculated for the pristine NUS-8/PIM-1 membrane (11).[33] This excellent selectivity is associated with a high CO_2 permeability (6700 barrer) that is very attractive for separation applications. Indeed, incorporating the functionalized NUS-8-CO_2H MOF into PIM-1 enables improvement of the selectivity of the membrane while maintaining a high flux characteristic of PIM-1 membranes.

We further explored the microscopic transport mechanism at the origin of this attractive separation performance. The separation mechanism can be classified as "solubility dominated" or "diffusivity dominated" depending on whether the separation is driven by a large difference between the calculated steady-state concentrations of the guest molecules or by a large difference between their calculated diffusivities within the MMM model. Figure 5b depicts the residence time distributions for CO_2 and N_2 along the membrane model. CO_2 is characterized by a slightly higher residence time than N_2, in line with stronger interactions between CO_2 and NUS-8-CO_2H/PIM-1 as revealed above by our GCMC simulations (see Figure 3). This difference is however not as marked as the difference in the steady-state concentration profiles of both molecules throughout the membrane shown in Figure 5a. Therefore, it is the difference between the solubilities that governs the separation rather than the difference between diffusivities. To quantify this, we calculated the solubility and diffusion contributions to the global selectivity by computing the ratio of the concentration profiles and the residence time distributions for each penetrant; these are shown in Figure 5c and Figure 5d, respectively. Indeed, the average solubility selectivity (43) is much higher than the average diffusion selectivity (0.7). In our previous study,[33] we have shown that the CO_2/N_2 selectivity is mainly solubility dominated for the pristine NUS-8/PIM-1 membrane, and we demonstrate here

https://doi.org/10.1021/acsami.2c00090
ACS Appl. Mater. Interfaces 2022, 14, 16820−16829

that this is also the case for the functionalized NUS-8-CO_2H/PIM-1 composite. Our results show that in a scheme of a solubility dominated separation mechanism, the performance of the membrane can be enhanced via the introduction of a CO_2-philic functionality in the MOF.

4. CONCLUSION

We have previously shown that the good CO_2/N_2 separation performance of NUS-8/PIM-1 was ascribed to (i) an increased adsorption selectivity of CO_2 molecules within the interfacial microvoids present in the composite and (ii) a solubility-driven separation mechanism. On the basis of these previous findings, we hypothesized that increasing the CO_2 affinity of the NUS-8 MOF by ligand functionalization while keeping a solubility-driven mechanism would enhance the separation performance of the corresponding MMM. We built an atomistic NUS-8-CO_2H/PIM-1 model and explored its separation and transport properties for the equimolar CO_2/N_2 gas mixture via equilibrium MD, CGMC, and CGD-MD simulations. These simulations supported the idea that in the case of a solubility-driven separation mechanism, the separation performance of the MMM can be improved by grafting a highly interacting chemical functionality in the organic linker of the MOF. The NUS-8-CO_2H/PIM-1 MMM provides an example of the success that can be achieved considering this strategy, as the CO_2/N_2 separation performance is remarkably improved by a factor of 3 while maintaining a relatively fast CO_2 permeability. We note that a very recent publication that appeared during the review process of this article[71] shows that it is feasible to synthesize NUS-8-CO_2H as well as its PIM-1-based MMM. Interestingly, the experimentally reported gas separation performance of the resulting MMM supports our theoretical predictions. This work highlights how deepening our understanding of the guest separation mechanism within MMMs at the molecular level can guide the rational development of membranes for societal and environmentally relevant applications.

■ ASSOCIATED CONTENT

Supporting Information

The Supporting Information is available free of charge at https://pubs.acs.org/doi/10.1021/acsami.2c00090.

Details of the force fields, LJ parameters, and partial charges, single-component CO_2 and N_2 adsorption isotherms of bulk NUS-8 and NUS-8-CO_2H, and simulation setup for the CGD-MD simulations (PDF)

■ AUTHOR INFORMATION

Corresponding Author

Rocio Semino − *ICGM, Université de Montpellier, CNRS, ENSCM, Montpellier 34293, France;* orcid.org/0000-0003-3937-7414; Email: rocio.semino@umontpellier.fr

Authors

Dong Fan − *ICGM, Université de Montpellier, CNRS, ENSCM, Montpellier 34293, France;* orcid.org/0000-0003-1873-3416

Aydin Ozcan − *ICGM, Université de Montpellier, CNRS, ENSCM, Montpellier 34293, France*

Naseem A. Ramsahye − *ICGM, Université de Montpellier, CNRS, ENSCM, Montpellier 34293, France*

Guillaume Maurin − *ICGM, Université de Montpellier, CNRS, ENSCM, Montpellier 34293, France*

Complete contact information is available at: https://pubs.acs.org/10.1021/acsami.2c00090

Author Contributions

†D.F. and A.O. contributed equally.

Notes

The authors declare no competing financial interest.

■ ACKNOWLEDGMENTS

This work benefited from the support of the project POCEMON ANR-18-CE05-0039 of the French National Research Agency (ANR) and the National Research Foundation Singapore (NRF). This work was granted access to the HPC resources of CINES under Allocation A0100907613 made by GENCI.

■ REFERENCES

(1) Qian, Q.; Asinger, P. A.; Lee, M. J.; Han, G.; Mizrahi Rodriguez, K.; Lin, S.; Benedetti, F. M.; Wu, A. X.; Chi, W. S.; Smith, Z. P. MOF-Based Membranes for Gas Separations. *Chem. Rev.* **2020**, *120*, 8161−8266.

(2) Liu, G.; Chernikova, V.; Liu, Y.; Zhang, K.; Belmabkhout, Y.; Shekhah, O.; Zhang, C.; Yi, S.; Eddaoudi, M.; Koros, W. J. Mixed Matrix Formulations with MOF Molecular Sieving for Key Energy-Intensive Separations. *Nat. Mater.* **2018**, *17*, 283−289.

(3) Robeson, L. M. The Upper Bound Revisited. *J. Membr. Sci.* **2008**, *320*, 390−400.

(4) Adams, R. T.; Lee, J. S.; Bae, T.-H.; Ward, J. K.; Johnson, J. R.; Jones, C. W.; Nair, S.; Koros, W. J. CO_2−CH_4 Permeation in High Zeolite 4A Loading Mixed Matrix Membranes. *J. Membr. Sci.* **2011**, *367*, 197−203.

(5) Li, X.; Ma, L.; Zhang, H.; Wang, S.; Jiang, Z.; Guo, R.; Wu, H.; Cao, X.; Yang, J.; Wang, B. Synergistic Effect of Combining Carbon Nanotubes and Graphene Oxide in Mixed Matrix Membranes for Efficient CO_2 Separation. *J. Membr. Sci.* **2015**, *479*, 1−10.

(6) Li, X.; Cheng, Y.; Zhang, H.; Wang, S.; Jiang, Z.; Guo, R.; Wu, H. Efficient CO_2 Capture by Functionalized Graphene Oxide Nanosheets as Fillers To Fabricate Multi-Permselective Mixed Matrix Membranes. *ACS Appl. Mater. Interfaces* **2015**, *7*, 5528−5537.

(7) Wang, B.; Sheng, M.; Xu, J.; Zhao, S.; Wang, J.; Wang, Z. Recent Advances of Gas Transport Channels Constructed with Different Dimensional Nanomaterials in Mixed-Matrix Membranes for CO_2 Separation. *Small Methods* **2020**, *4*, 1900749.

(8) Pinto, R. V.; Wang, S.; Tavares, S. R.; Pires, J.; Antunes, F.; Vimont, A.; Clet, G.; Daturi, M.; Maurin, G.; Serre, C.; Pinto, M. L. Tuning Cellular Biological Functions Through the Controlled Release of NO from a Porous Ti-MOF. *Angew. Chem.* **2020**, *132*, 5173−5181.

(9) Zhou, S.; Shekhah, O.; Jia, J.; Czaban-Jóźwiak, J.; Bhatt, P. M.; Ramírez, A.; Gascon, J.; Eddaoudi, M. Electrochemical Synthesis of Continuous Metal−Organic Framework Membranes for Separation of Hydrocarbons. *Nat. Energy* **2021**, *6*, 882−891.

(10) Jiang, H.; Alezi, D.; Eddaoudi, M. A Reticular Chemistry Guide for the Design of Periodic Solids. *Nat. Rev. Mater.* **2021**, *6*, 466−487.

(11) Seoane, B.; Coronas, J.; Gascon, I.; Benavides, M. E.; Karvan, O.; Caro, J.; Kapteijn, F.; Gascon, J. Metal−Organic Framework Based Mixed Matrix Membranes: A Solution for Highly Efficient CO_2 Capture? *Chem. Soc. Rev.* **2015**, *44*, 2421−2454.

(12) Knebel, A.; Bavykina, A.; Datta, S. J.; Sundermann, L.; Garzon-Tovar, L.; Lebedev, Y.; Durini, S.; Ahmad, R.; Kozlov, S. M.; Shterk, G.; Karunakaran, M.; Carja, I. D.; Simic, D.; Weilert, I.; Klüppel, M.; Giese, U.; Cavallo, L.; Rueping, M.; Eddaoudi, M.; Caro, J.; Gascon, J. Solution Processable Metal−Organic Frameworks for Mixed Matrix Membranes Using Porous Liquids. *Nat. Mater.* **2020**, *19*, 1346−1353.

(13) Lee, T. H.; Ozcan, A.; Park, I.; Fan, D.; Jang, J. K.; Mileo, P. G. M.; Yoo, S. Y.; Roh, J. S.; Kang, J. H.; Lee, B. K.; Cho, Y. H.; Semino, R.; Kim, H. W.; Maurin, G.; Park, H. B. Disclosing the Role of Defect-Engineered Metal−Organic Frameworks in Mixed Matrix Membranes for Efficient CO_2 Separation: A Joint Experimental-Computational Exploration. *Adv. Funct. Mater.* **2021**, *31*, 2103973.
(14) Shan, M.; Liu, X.; Wang, X.; Yarulina, I.; Seoane, B.; Kapteijn, F.; Gascon, J. Facile Manufacture of Porous Organic Framework Membranes for Precombustion CO_2 Capture. *Sci. Adv.* **2018**, *4*, No. eaau1698.
(15) Lee, T. H.; Jung, J. G.; Kim, Y. J.; Roh, J. S.; Yoon, H. W.; Ghanem, B. S.; Kim, H. W.; Cho, Y. H.; Pinnau, I.; Park, H. B. Defect Engineering in Metal−Organic Frameworks Towards Advanced Mixed Matrix Membranes for Efficient Propylene/Propane Separation. *Angew. Chem.* **2021**, *133*, 13191−13198.
(16) He, S.; Zhu, B.; Jiang, X.; Han, G.; Li, S.; Lau, C. H.; Wu, Y.; Zhang, Y.; Shao, L. Symbiosis-Inspired de Novo Synthesis of Ultrahigh MOF Growth Mixed Matrix Membranes for Sustainable Carbon Capture. *Proc. Natl. Acad. Sci. U.S.A.* **2022**, *119*, No. e2114964119.
(17) He, S.; Jiang, X.; Li, S.; Ran, F.; Long, J.; Shao, L. Intermediate Thermal Manipulation of Polymers of Intrinsic Microporous (PIMS) Membranes for Gas Separations. *AIChE J.* **2020**, *66*, No. e16543.
(18) Forgan, R. S. The Surface Chemistry of Metal−Organic Frameworks and Their Applications. *Dalton Trans.* **2019**, *48*, 9037−9042.
(19) Venna, S. R.; Lartey, M.; Li, T.; Spore, A.; Kumar, S.; Nulwala, H. B.; Luebke, D. R.; Rosi, N. L.; Albenze, E. Fabrication of MMMs with Improved Gas Separation Properties Using Externally-Functionalized MOF Particles. *J. Mater. Chem. A* **2015**, *3*, 5014−5022.
(20) Tien-Binh, N.; Vinh-Thang, H.; Chen, X. Y.; Rodrigue, D.; Kaliaguine, S. Polymer Functionalization to Enhance Interface Quality of Mixed Matrix Membranes for High CO_2/CH_4 Gas Separation. *J. Mater. Chem. A* **2015**, *3*, 15202−15213.
(21) Carja, I.-D.; Tavares, S. R.; Shekhah, O.; Ozcan, A.; Semino, R.; Kale, V. S.; Eddaoudi, M.; Maurin, G. Insights into the Enhancement of MOF/Polymer Adhesion in Mixed-Matrix Membranes *via* Polymer Functionalization. *ACS Appl. Mater. Interfaces* **2021**, *13*, 29041−29047.
(22) Ghalei, B.; Sakurai, K.; Kinoshita, Y.; Wakimoto, K.; Isfahani, A. P.; Song, Q.; Doitomi, K.; Furukawa, S.; Hirao, H.; Kusuda, H.; Kitagawa, S.; Sivaniah, E. Enhanced Selectivity in Mixed Matrix Membranes for CO_2 Capture through Efficient Dispersion of Amine-Functionalized MOF Nanoparticles. *Nat. Energy* **2017**, *2*, 17086.
(23) Sabetghadam, A.; Seoane, B.; Keskin, D.; Duim, N.; Rodenas, T.; Shahid, S.; Sorribas, S.; Guillouzer, C. L.; Clet, G.; Tellez, C.; Daturi, M.; Coronas, J.; Kapteijn, F.; Gascon, J. Metal Organic Framework Crystals in Mixed-Matrix Membranes: Impact of the Filler Morphology on the Gas Separation Performance. *Adv. Funct. Mater.* **2016**, *26*, 3154−3163.
(24) Rodenas, T.; van Dalen, M.; García-Pérez, E.; Serra-Crespo, P.; Zornoza, B.; Kapteijn, F.; Gascon, J. Visualizing MOF Mixed Matrix Membranes at the Nanoscale: Towards Structure-Performance Relationships in CO_2/CH_4 Separation Over NH_2 -MIL-53(Al)@PI. *Adv. Funct. Mater.* **2014**, *24*, 249−256.
(25) Dechnik, J.; Gascon, J.; Doonan, C. J.; Janiak, C.; Sumby, C. J. Mixed-Matrix Membranes. *Angew. Chem., Int. Ed.* **2017**, *56*, 9292−9310.
(26) Wang, Z.; Ren, H.; Zhang, S.; Zhang, F.; Jin, J. Polymers of Intrinsic Microporosity/Metal−Organic Framework Hybrid Membranes with Improved Interfacial Interaction for High-Performance CO_2 Separation. *J. Mater. Chem. A* **2017**, *5*, 10968−10977.
(27) Ahmad, M. Z.; Navarro, M.; Lhotka, M.; Zornoza, B.; Téllez, C.; de Vos, W. M.; Benes, N. E.; Konnertz, N. M.; Visser, T.; Semino, R.; Maurin, G.; Fila, V.; Coronas, J. Enhanced Gas Separation Performance of 6FDA-DAM Based Mixed Matrix Membranes by Incorporating MOF UiO-66 and Its Derivatives. *J. Membr. Sci.* **2018**, *558*, 64−77.
(28) Ma, X.; Swaidan, R. J.; Wang, Y.; Hsiung, C.; Han, Y.; Pinnau, I. Highly Compatible Hydroxyl-Functionalized Microporous Polyimide-ZIF-8 Mixed Matrix Membranes for Energy Efficient Propylene/Propane Separation. *ACS Appl. Nano Mater.* **2018**, *1*, 3541−3547.
(29) Liu, B.; Li, D.; Yao, J.; Sun, H. Enhanced CO_2 Selectivity of Polyimide Membranes through Dispersion of Polyethyleneimine Decorated UiO-66 Particles. *J. Appl. Polym. Sci.* **2020**, *137*, 49068.
(30) Park, H. B.; Kamcev, J.; Robeson, L. M.; Elimelech, M.; Freeman, B. D. Maximizing the Right Stuff: The Trade-off between Membrane Permeability and Selectivity. *Science* **2017**, *356*, No. eaab0530.
(31) Amedi, H. R.; Aghajani, M. Aminosilane-Functionalized ZIF-8/PEBA Mixed Matrix Membrane for Gas Separation Application. *Microporous Mesoporous Mater.* **2017**, *247*, 124−135.
(32) Pu, Y.; Yang, Z.; Wee, V.; Wu, Z.; Jiang, Z.; Zhao, D. Amino-Functionalized NUS-8 Nanosheets as Fillers in PIM-1 Mixed Matrix Membranes for CO_2 Separations. *J. Membr. Sci.* **2022**, *641*, 119912.
(33) Fan, D.; Ozcan, A.; Ramsahye, N. A.; Zhao, D.; Maurin, G.; Semino, R. Is Porosity at the MOF/Polymer Interface Necessarily an Obstacle to Optimal Gas-Separation Performances in Mixed Matrix Membranes? *ACS Mater. Lett.* **2021**, *3*, 344−350.
(34) Hwang, S.; Semino, R.; Seoane, B.; Zahan, M.; Chmelik, C.; Valiullin, R.; Bertmer, M.; Haase, J.; Kapteijn, F.; Gascon, J.; Maurin, G.; Kärger, J. Revealing the Transient Concentration of CO_2 in a Mixed-Matrix Membrane by IR Microimaging and Molecular Modeling. *Angew. Chem., Int. Ed.* **2018**, *57*, 5156−5160.
(35) Mizrahi Rodriguez, K.; Wu, A. X.; Qian, Q.; Han, G.; Lin, S.; Benedetti, F. M.; Lee, H.; Chi, W. S.; Doherty, C. M.; Smith, Z. P. Facile and Time-Efficient Carboxylic Acid Functionalization of PIM-1: Effect on Molecular Packing and Gas Separation Performance. *Macromolecules* **2020**, *53*, 6220−6234.
(36) Semino, R.; Ramsahye, N. A.; Ghoufi, A.; Maurin, G. Microscopic Model of the Metal−Organic Framework/Polymer Interface: A First Step toward Understanding the Compatibility in Mixed Matrix Membranes. *ACS Appl. Mater. Interfaces* **2016**, *8*, 809−819.
(37) Hutter, J.; Iannuzzi, M.; Schiffmann, F.; VandeVondele, J. CP2K: Atomistic Simulations of Condensed Matter Systems. *WIREs Comput. Mol. Sci.* **2014**, *4*, 15−25.
(38) Perdew, J. P.; Burke, K.; Ernzerhof, M. Generalized Gradient Approximation Made Simple. *Phys. Rev. Lett.* **1996**, *77*, 3865−3868.
(39) VandeVondele, J.; Hutter, J. Gaussian Basis Sets for Accurate Calculations on Molecular Systems in Gas and Condensed Phases. *J. Chem. Phys.* **2007**, *127*, 114105.
(40) Goedecker, S.; Teter, M.; Hutter, J. Separable Dual-Space Gaussian Pseudopotentials. *Phys. Rev. B* **1996**, *54*, 1703−1710.
(41) Hartwigsen, C.; Goedecker, S.; Hutter, J. Relativistic Separable Dual-Space Gaussian Pseudopotentials from H to Rn. *Phys. Rev. B* **1998**, *58*, 3641−3662.
(42) Krack, M. Pseudopotentials for H to Kr Optimized for Gradient-Corrected Exchange-Correlation Functionals. *Theor. Chem. Acc.* **2005**, *114*, 145−152.
(43) Grimme, S. Semiempirical GGA-type density functional constructed with a long-range dispersion correction. *J. Comput. Chem.* **2006**, *27*, 1787−1799.
(44) Cheng, Y.; Tavares, S. R.; Doherty, C. M.; Ying, Y.; Sarnello, E.; Maurin, G.; Hill, M. R.; Li, T.; Zhao, D. Enhanced Polymer Crystallinity in Mixed-Matrix Membranes Induced by Metal−Organic Framework Nanosheets for Efficient CO_2 Capture. *ACS Appl. Mater. Interfaces* **2018**, *10*, 43095−43103.
(45) Campañá, C.; Mussard, B.; Woo, T. K. Electrostatic Potential Derived Atomic Charges for Periodic Systems Using a Modified Error Functional. *J. Chem. Theory Comput.* **2009**, *5*, 2866−2878.
(46) Kühne, T. D.; Iannuzzi, M.; Del Ben, M.; Rybkin, V. V.; Seewald, P.; Stein, F.; Laino, T.; Khaliullin, R. Z.; Schütt, O.; Schiffmann, F.; Golze, D.; Wilhelm, J.; Chulkov, S.; Bani-Hashemian, M. H.; Weber, V.; Borštnik, U.; Taillefumier, M.; Jakobovits, A. S.; Lazzaro, A.; Pabst, H.; Müller, T.; Schade, R.; Guidon, M.; Andermatt, S.; Holmberg, N.; Schenter, G. K.; Hehn, A.; Bussy, A.;

https://doi.org/10.1021/acsami.2c00090
ACS Appl. Mater. Interfaces 2022, 14, 16820−16829

Belleflamme, F.; Tabacchi, G.; Glöß, A.; Lass, M.; Bethune, I.; Mundy, C. J.; Plessl, C.; Watkins, M.; VandeVondele, J.; Krack, M.; Hutter, J. CP2K: An Electronic Structure and Molecular Dynamics Software Package - Quickstep: Efficient and Accurate Electronic Structure Calculations. *J. Chem. Phys.* **2020**, *152*, 194103.
(47) Yu, J.; Xie, L.-H.; Li, J.-R.; Ma, Y.; Seminario, J. M.; Balbuena, P. B. CO_2 Capture and Separations Using MOFs: Computational and Experimental Studies. *Chem. Rev.* **2017**, *117*, 9674−9754.
(48) Rappe, A. K.; Casewit, C. J.; Colwell, K. S.; Goddard, W. A.; Skiff, W. M. UFF, a Full Periodic Table Force Field for Molecular Mechanics and Molecular Dynamics Simulations. *J. Am. Chem. Soc.* **1992**, *114*, 10024−10035.
(49) Semino, R.; Moreton, J. C.; Ramsahye, N. A.; Cohen, S. M.; Maurin, G. Understanding the Origins of Metal−Organic Framework/Polymer Compatibility. *Chem. Sci.* **2018**, *9*, 315−324.
(50) Larsen, G. S.; Lin, P.; Hart, K. E.; Colina, C. M. Molecular Simulations of PIM-1-like Polymers of Intrinsic Microporosity. *Macromolecules* **2011**, *44*, 6944−6951.
(51) Ozcan, A.; Semino, R.; Maurin, G.; Yazaydin, A. O. Modeling of Gas Transport through Polymer/MOF Interfaces: A Microsecond-Scale Concentration Gradient-Driven Molecular Dynamics Study. *Chem. Mater.* **2020**, *32*, 1288−1296.
(52) Berendsen, H. J. C.; Postma, J. P. M.; van Gunsteren, W. F.; DiNola, A.; Haak, J. R. Molecular Dynamics with Coupling to an External Bath. *J. Chem. Phys.* **1984**, *81*, 3684−3690.
(53) Todorov, I. T.; Smith, W.; Trachenko, K.; Dove, M. T. DL_POLY_3: New Dimensions in Molecular Dynamics Simulations via Massive Parallelism. *J. Mater. Chem.* **2006**, *16*, 1911.
(54) Lorentz, H. A. Ueber die Anwendung des Satzesvom Virial in der kinetischenTheorie der Gase. *Ann. Phys.* **1881**, *248*, 127−136.
(55) Ewald, P. P. Die Berechnungoptischer und elektrostatischer-Gitterpotentiale. *Ann. Phys.* **1921**, *369*, 253−287.
(56) Willems, T. F.; Rycroft, C. H.; Kazi, M.; Meza, J. C.; Haranczyk, M. Algorithms and Tools for High-Throughput Geometry-Based Analysis of Crystalline Porous Materials. *Microporous Mesoporous Mater.* **2012**, *149*, 134−141.
(57) Dubbeldam, D.; Calero, S.; Ellis, D. E.; Snurr, R. Q. RASPA: Molecular Simulation Software for Adsorption and Diffusion in Flexible Nanoporous Materials. *Mol. Simul.* **2016**, *42*, 81−101.
(58) Harris, J. G.; Yung, K. H. Carbon Dioxide's Liquid-Vapor Coexistence Curve And Critical Properties as Predicted by a Simple Molecular Model. *J. Phys. Chem.* **1995**, *99*, 12021−12024.
(59) Potoff, J. J.; Siepmann, J. I. Vapor−Liquid Equilibria of Mixtures Containing Alkanes, Carbon Dioxide, and Nitrogen. *AIChE J.* **2001**, *47*, 1676−1682.
(60) Vlugt, T. J. H.; García-Pérez, E.; Dubbeldam, D.; Ban, S.; Calero, S. Computing the Heat of Adsorption Using Molecular Simulations: The Effect of Strong Coulombic Interactions. *J. Chem. Theory Comput.* **2008**, *4*, 1107−1118.
(61) Abraham, M. J.; Murtola, T.; Schulz, R.; Páll, S.; Smith, J. C.; Hess, B.; Lindahl, E. GROMACS: High Performance Molecular Simulations through Multi-Level Parallelism from Laptops to Supercomputers. *SoftwareX* **2015**, *1−2*, 19−25.
(62) Tribello, G. A.; Bonomi, M.; Branduardi, D.; Camilloni, C.; Bussi, G. PLUMED 2: New Feathers for an Old Bird. *Comput. Phys. Commun.* **2014**, *185*, 604−613.
(63) Hu, Z.; Chen, Y.; Jiang, J. ZeoliticImidazolate Framework-8 as a Reverse Osmosis Membrane for Water Desalination: Insight from Molecular Simulation. *J. Chem. Phys.* **2011**, *134*, 134705.
(64) Raju, M.; Govindaraju, P. B.; van Duin, A. C. T.; Ihme, M. Atomistic and Continuum Scale Modeling of Functionalized Graphyne Membranes for Water Desalination. *Nanoscale* **2018**, *10*, 3969−3980.
(65) Nosé, S. A Unified Formulation of the Constant Temperature Molecular Dynamics Methods. *J. Chem. Phys.* **1984**, *81*, 511−519.
(66) Basconi, J. E.; Shirts, M. R. Effects of Temperature Control Algorithms on Transport Properties and Kinetics in Molecular Dynamics Simulations. *J. Chem. Theory Comput.* **2013**, *9*, 2887−2899.
(67) Essmann, U.; Perera, L.; Berkowitz, M. L.; Darden, T.; Lee, H.; Pedersen, L. G. A Smooth Particle Mesh Ewald Method. *J. Chem. Phys.* **1995**, *103*, 8577−8593.
(68) Ozcan, A.; Perego, C.; Salvalaglio, M.; Parrinello, M.; Yazaydin, O. Concentration Gradient Driven Molecular Dynamics: A New Method for Simulations of Membrane Permeation and Separation. *Chem. Sci.* **2017**, *8*, 3858−3865.
(69) Myers, A. L.; Monson, P. A. Adsorption in Porous Materials at High Pressure: Theory and Experiment. *Langmuir* **2002**, *18*, 10261−10273.
(70) Sarkisov, L.; Harrison, A. Computational Structure Characterisation Tools in Application to Ordered and Disordered Porous Materials. *Mol. Simul.* **2011**, *37*, 1248−1257.
(71) Wang, D.; Ying, Y.; Zheng, Y.; Pu, Y.; Yang, Z.; Zhao, D. Induced Polymer Crystallinity in Mixed Matrix Membranes by Metal-Organic Framework Nanosheets for Gas Separation. *J. Membr. Sci. Lett.* **2022**, *2*, 100017.

Recommended by ACS

Hierarchical Metal–Organic Aerogel as a Highly Selective and Sustainable CO_2 Adsorbent
Heehyeon Lee, Seok Min Yoon, *et al.*
OCTOBER 06, 2022
ACS APPLIED MATERIALS & INTERFACES
READ

Hierarchical Amine-Functionalized ZIF-8 Mixed-Matrix Membranes with an Engineered Interface and Transport Pathway for Efficient Gas Separation
Jin Hui Jo, Won Seok Chi, *et al.*
AUGUST 08, 2022
ACS APPLIED POLYMER MATERIALS
READ

Fine Tuning the Pore Surface in Zirconium Metal–Organic Frameworks for Selective Ethane/Ethylene Separation
Yuchen Hu, Jian Zhang, *et al.*
OCTOBER 14, 2022
ACS APPLIED ENGINEERING MATERIALS
READ

Comparative Studies on the Proton Conductivities of Hafnium-Based Metal–Organic Frameworks and Related Chitosan or Nafion Composite Membranes
Hui-Min Ren, Gang Li, *et al.*
JUNE 14, 2022
INORGANIC CHEMISTRY
READ

Get More Suggestions >

https://doi.org/10.1021/acsami.2c00090
ACS Appl. Mater. Interfaces 2022, 14, 16820−16829